

Directionality of Tonal Components of Ship Noise Using Arctic Hydrophone Array Elements

Dugald J. M. Thomson[✉], Member, IEEE, and David R. Barclay[✉], Member, IEEE

Abstract—The horizontal directionality of ship-radiated noise was estimated in the Canadian Arctic Archipelago using two 48-element bottom-mounted hydrophone arrays. Source levels (SL) were estimated using automated identification system data for distance and bearing with a geometric spreading propagation loss model for ships passing within 3 km of the arrays. Time-averaged received levels are calculated in 3-s increments for broadband (10–600 Hz) as well as selected narrowband tonal sources. Tonal components are identified with spectral analysis and algorithmically tracked in the time-frequency domain. From the difference of received levels and propagation loss, SLs are calculated and sorted by ship's bearing from each of the 96 array elements for both broadband and predominant narrowband sources. Broadband SL estimates ranged from 148 to 181 dB re 1 $\mu\text{Pa}^2 \text{m}^{-2}$ for the four ships of opportunity.

Index Terms—Arctic acoustics, noise directionality, propeller tonals, ship detection, ship noise, source level (SL) estimation, underwater radiated noise (URN).

I. INTRODUCTION

UNDERWATER radiated noise (URN) from ships has been studied across a diverse scientific field, studying anthropogenic contributions [1], [2] as a pollutant and its resultant effects on the ocean [3], [4]. This source can be a significant contributor to ambient noise levels [5], particularly in acoustically pristine areas such as the Arctic [6], [7], [8]. Ocean noise affects marine fauna [9], [10] with impacts ranging from behavioral disturbance [11], [12], [13], [14] to physiological effects [15], [16], and is attracting regulatory action and management planning in many jurisdictions [17], [18]. Mitigative measures such as vessel slowdowns have been shown to be effective [19] at reducing noise levels.

Ocean ambient noise levels are sensitive to shipping noise at both distant and close ranges, with the former contributing continuously to the background noise level between a few Hz and a few thousand Hz [20]. Ship detection and classification using underwater acoustics has been an important research theme with a long history of military [21], [22], [23] and more recently biological and ecological monitoring applications [24], [25], [26]. Modern navies regularly send their ships through an acoustic ranging process to provide a detailed characterization

Received 30 April 2024; revised 1 December 2024; accepted 26 February 2025. This work was supported by the Canadian Department of National Defence. (*Corresponding author: Dugald J. M. Thomson.*)

Associate Editor: A. Hunter.

The authors are with the Department of Oceanography, Dalhousie University, Halifax, NS B3H 4R2, Canada (e-mail: dugald@dal.ca; dbarclay@dal.ca). Digital Object Identifier 10.1109/JOE.2025.3553955

1558-1691 © 2025 IEEE. All rights reserved, including rights for text and data mining, and training of artificial intelligence and similar technologies. Personal use is permitted, but republication/redistribution requires IEEE permission. See <https://www.ieee.org/publications/rights/index.html> for more information.

of the acoustic signature [27] under a range of conditions, aiming to isolate the contributions from individual sound-producing components such as pumps and generators, identify tactical acoustic vulnerabilities, and determine a cavitation inception speed (CIS). In the biological realm, the sound exposure level (SEL) is a useful metric for ascertaining a time-weighted sound energy exposure caused by a noise source. The probability distribution function of SEL has been used for mapping vessel noise and identifying areas of ecological concern [28], such as the Arctic, where ship-related noise may be increasing at greater than 3 dB/decade [29].

Accurately predicting ship noise requires well-characterized radiated noise models [30], [31], [32], for which standards have been developed [33], [34], [35]. The models described by these standards are suitable for most applications but neglect horizontal directionality. Ships are complex sources of underwater noise. The diverse hydrodynamic and mechanical noise sources are spread across the length of a ship, radiating into the water with considerable variability in the horizontal.

Acoustic modeling, whether for estimating propagation from a known source or assessing ambient noise characteristics, requires a general understanding of how noise radiates from the source, and propagates into the water column; this is a prerequisite for predicting the noise contribution of individual ships, improving the fidelity of operational noise models, and understanding noise impacts on the environment. This study uses a 96-element horizontal line array (HLA) to measure the directional and spectral characteristics of vessels of opportunity. This article will describe a technique for estimating the horizontal directionality of radiated ship noise, for both broadband and narrowband frequency components.

II. SHIP RADIATED NOISE

The URN measured at a nearby receiver results from: 1) ship-dependent factors such as the ship's idiosyncratic characteristics (e.g., engine type), operating mode (e.g., number of engines engaged), propeller fit, speed, and maintenance status; and 2) ship-independent variables such as the natural background noise, secondary contacts, water column properties, and seabed and receiver characteristics. The main sources of ship-related noise are the propulsion machinery and propulsor [36], [37].

A. Ship Noise Spectrum

Every ship has a unique acoustic spectral signature that depends on characteristics such as engine type and propulsion

system, speed and machinery state, and maintenance status [38]. Noise spectra components can be broadband or tonal; broadband sources have a continuous spectrum and tend to be related to hydrodynamics, such as cavitation or flow noise, whereas tonal components have a discrete frequency, often with harmonics, and tend to be related to the following:

- 1) a ship's propulsion system;
- 2) prime mover (engine);
- 3) electrical and auxiliary machinery.

1) *Tonal Components of URN*: Most large ships employ a type of diesel engine configuration and as such, have some common features, foremost the cylinder firing rate (CFR, in Hz) and its many harmonics. A CFR is caused by combustion in a 2- or 4-stroke engine [37] and will appear as a series of tonal harmonics across the low-frequency ($\sim < 300$ Hz) spectrum with the fundamental rate corresponding to the CFR of a single cylinder. The combustion cycle for a four-stroke engine is 1) intake, 2) compression, 3) power, and 4) exhaust, and each stage of this cycle occurs once every two crankshaft revolutions (CSR = $2 \times$ CFR). A two-stroke engine combines the intake and exhaust cycles such that the crankshaft turns once per cycle (CSR = CFR). Prominence describes the tonality of a discrete URN source and is defined by the amplitude of the tonal compared to the amplitude of the noise at the neighboring frequencies. The engine firing rate, EFR = $N_c \times$ CFR, can in some cases be noted in the spectrum based on relative prominence within the CFR harmonic structure at harmonics corresponding to the number of cylinders, N_c . CSR is equivalent to engine output speed in rotations per minute (ERPM), which is controlled from the ships' bridge or engine room. Diesel engines are categorized according to their ERPM; high-speed engines operate > 1000 ERPM, medium-speed engines 300–1000 ERPM, and low-speed engines < 300 ERPM, with most marine engines falling in the latter two categories.

2) *Spectral Characteristics of Tones*: Tones in ship signatures may result from a variety of shipborne sources including propulsion and machinery and tend to be more prominent in the spectrum as they often exhibit higher sound levels compared to the surrounding broadband noise at the same frequencies [39]. Narrowband spectral analysis of a typical commercial ship [38], identified engine-, blade-, and generator-related sources in 0.5-Hz bands at low and maximum speed. This work identified several characteristics of the three distinct noise sources, including the relative stability in amplitude and frequency of engine-related tonals as compared to those related to propulsion, the speed-dependence of relative amplitudes between the three sources, and the directionality, where low frequencies (< 25 Hz) tended to radiate noise omnidirectional in azimuth, whereas higher frequencies (340–360 Hz) directivity is reduced fore and aft, attributed to hull and bubble wake attenuation of the radiated noise.

The engine crankshaft powers the propulsion, typically through one or more propellers each mounted to a shaft through a gearset with reduction ratio R_r , where the propeller shaft rate

$$\text{SR} = R_r \times \text{CSR}. \quad (1)$$

Other common propulsion configurations include direct-drive, where there is no reduction gearing ($R_r = 1$), and SR = CSR, and ac or dc electric motors which power a propeller shaft or thruster that is not directly mechanically coupled to the crankshaft. Auxiliary machinery can also be powered by the main engines, and these may have a vibrational rate that will appear in the spectrum as one or more discrete tonals at some multiple of the CFR. Generator tonals tend to show high-frequency stability compared to propulsion-related sources, particularly during maneuvers or high sea states when the speed controller fluctuates, which is more apparent at higher frequencies or processing resolutions.

The number of blades N_b is an important characteristic in propeller design, with most marine propellers having 3–7 blades, and it is useful to define the blade rate, the frequency at which a blade passes the top center of the propeller radius, as

$$\text{BR} = N_b \times \text{SR}. \quad (2)$$

3) *Propeller Cavitation*: When a ship's propeller develops sufficient pressure gradients across its surfaces due to its rotational speed, a process of bubble collapse known as cavitation can occur, which creates a powerful and broadband noise source that may dominate a ship's acoustic signature. Models have been developed [40] to account for this effect, which can extend through the acoustic spectrum to 100 kHz when the ship is propelled above its CIS. Repeat measurements of a single ship found that turning maneuvers could add up to 10 dB to the ship's broadband SL due to enhanced cavitation, further evidenced by propeller blade rate modulation during these measurements [41]. Below CIS, a ship's acoustic signature is composed primarily of the tonal sources associated with machinery, whereas above CIS broadband noise and blade rate harmonics may dominate, particularly at the fundamental blade rate and its first harmonics [41].

B. Source Levels

Ainslie et al. [42] provided a thorough overview of the established standards [33], [34], [35], which standardize the terminology and methods related to the measurement of ship noise. Radiated noise level (RNL, symbol L_{RN}), is defined by ISO 17208-1 [35] as a "measure of the underwater noise radiated by a surface vessel, obtained by averaging the far-field sound pressure level and scaling this quantity according to spherical spreading to a standard reference distance of 1 m." It is distinct from source level (SL, symbol L_s), which requires the determination of the propagation loss (PL, symbol N_{PL}), and thus can be difficult to calculate accurately, particularly in shallow water [42]. The difference in levels, $\Delta L = L_{RN} - L_s$, is defined by the formula in ISO 17208-2. Ainslie et al. discussed this difference for a 4-m source in deep water, noting that it ranged between -15 dB and $+5$ dB in the frequency range of 10–1000 Hz, with the difference represented by a dipole to monopole source factor dependent on the vertical measurement angles [42]. A modeling study estimated ship SL from acoustic time series, automated identification system (AIS) data, and a wavenumber integration PL model, and compared the ensemble

average of over 2000 ship passes to published SL across 4 categories of ships [43]. The study found a roughly 20 dB spread between the 1st and 99th percentile SL estimates of different detections of the same vessels, between 200 and 1000 Hz. More recently, ship SLs were estimated in shallow water using trans-dimensional Bayesian marginalization, with a technique using the Bayesian Information Criterion to optimize the density of ship noise source model points; SL uncertainties were found to be 3.2 dB/Hz for narrowband (between 20 and 120 Hz), and 1.8 dB/Hz for broadband (between 190 and 590 Hz) [44].

1) *Source Level Models*: A review of multiple studies of ship noise [45] found that ship speed and size were the factors most correlated to broadband SL, with mean broadband SL for most ships concentrated between 180 and 190 dB re 1 μPa , with passenger ships 6 dB quieter than the mean. This analysis provided a comparison of different ship noise studies and suggested that the ship noise field would benefit from increased attention to narrowband URN measurements, over broadband. Their meta-analysis produced an aggregate broadband SL model for passenger ships referred to here as the Chion model

$$L_S = 147.94 \text{ dB} + 15.39 \text{ dB} \times \log_{10} \left[\frac{\text{speed}}{1 \text{ knot}} \right] + 12.03 \text{ dB} \times \log_{10} \left[\frac{\text{width}}{1 \text{ m}} \right] - 4.83 \text{ dB} \times \left[\frac{\text{range}}{1 \text{ nm}} \right]. \quad (3)$$

Models have reliably predicted source SL using a range of predictors [39] related to ship design (such as length, draft, and age), operating parameters (speed, range, and secondary contacts), and oceanographic conditions (wind speed and wave height), where the variance between individual detections of the same ship often exceeded 10 dB. Other models have been proposed to account for the varying nature of signatures of individual ships [46] based on representing the ship as a surface monopole source. Earlier work from the US Navy's Naval Research Lab [32] proposed an update to a classical model for determining the ensemble spectra based on a power-law relationship of ship speed and length, which was instead based on a rational spectrum with parameters that are based on the ship noise spectra rather than physical parameters of the ship.

Estimating effective source depth also becomes an important problem when modeling PL. An accepted estimate [47] for effective source depth for a propeller was calculated by subtracting a proportion of the propeller diameter from the ship draft. The spectral characteristics of individual ships with controllable pitch propellers have been modeled [48] to try to predict the noise contribution of an individual vessel, based on the speed and pitch of the propeller. An empirical model was established to predict the spectral characteristics including broadband URN and shape of the propeller noise spectrum.

An alternative approach to estimating URN from an offboard receiver is to measure the onboard vibrations and develop a transfer function to estimate the in-water radiated noise. The efficacy of this approach has been demonstrated using onboard pressure sensors and accelerometers, correlated to measurements by offboard hydrophones [49]. To monitor the level of

noise radiated from a ship's propeller in real time, a Defense Research and Development Canada (DRDC) group equipped a naval training vessel with an accelerometer-based onboard sensor package and conducted controlled experiments at various speeds to determine the CIS [41]. The resultant model has been used to optimize propeller design for noise minimization.

C. Doppler Effect

Tracking tonal components as they shift in frequency due to the Doppler effect or mechanical changes in the ship has been identified as a challenge [50] in estimating SL. In the case of the Doppler effect, the shift in frequency can be used to estimate the ship speed using the relationship

$$\Delta f = f_c (\text{vcos}\theta) / c \quad (4)$$

where Δf is the observed shift, in Hz, $\text{vcos}\theta$ is the relative velocity between source and receiver, f_c is the center frequency of the discrete tonal, and c is the speed of sound. For a ship passing directly above a receiver from a relative bearing of -90° to 90° on a steady heading, the maximum Doppler shift is then

$$\Delta f = (2vf_c) / c. \quad (5)$$

The error in estimating the levels of a tone due to Doppler shift depends on the ratio of the total shift to the filter bandwidth, B [51], [51]. If this ratio is less than 1, then the error is negligible. However, if this ratio is greater than 1, then the error can be significant. The approximate formula for calculating the error in decibels is $10 \log(\Delta f / B)$, equating to 10 dB of error when estimating 1-Hz band levels for a ship passing directly over a receiver at 10 m/s measured at 750 Hz. This error source is generally addressed through averaging or widening processing bands to ensure the entire signal is captured.

URN tends to increase with propeller speed, research has compared the broadband signature of the same vessel with different propeller speeds and pitches [48], fitting an empirical noise model. Using a horizontal array to estimate the SL of narrowband tonals observed on distant vessels, the prominence of tonal components in the acoustic signatures was found to be 10–30 dB above local broadband noise levels [52]. When relying on standard methods using 1/3-octave averaging for assessing ship noise, tonals have the potential to distort evaluations of the effects of ship-generated noise.

D. Ship Noise Directionality

Inferring the direction from which underwater noise originates has been widely studied in the open literature (e.g., array processing), but the directionality of noise radiating from a ship has received less attention outside naval signature management circles. Noise directionality was estimated [53] for container ships passing an optimally configured deep water observatory near California; vertical arrays of high-frequency hydrophones were deployed along either side of a shipping channel at depths between 131 m and 565 m to provide ANSI [33] and ISO [35] compliance. The author proposes a method for isolating the radiated noise directionality at discrete frequencies using both a surface-corrected and surface-affected PL model, with

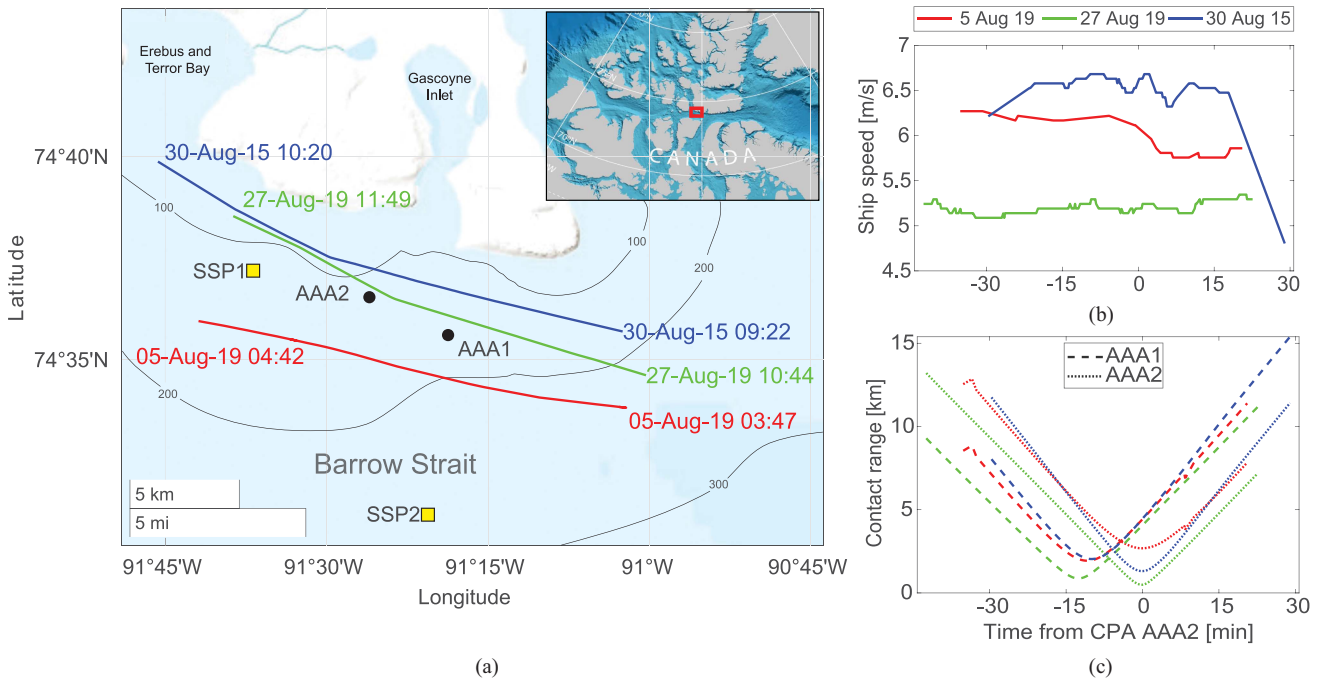


Fig. 1. AIS (a) track, (b) speed, and (c) contact range from the center of AAA1 and AAA2 for the Ocean Endeavour closest-point-of-approach on August 30, 2015 (blue) and 5 (red) and 30 August 2019 (green).

broadband RNL discrepancies reduced by up to 8 dB for the latter. This study used very low-frequency sources associated with the fundamental blade rate frequency (B1) and the fourth harmonic of CFR (C4). Asymmetries in RNL were found for both sources, with the B1 showing heightened RNL at the stern aspect as well as the starboard side, the latter radiation pattern attributed to the clockwise propeller rotation. C4 showed higher noise levels from the port aspect. The surface-corrected PL model relied on optimizing effective source depth by calculating the spectral differences in RL between hydrophones at different elevation angles.

Park et al. [55] examined the source spectra of a small vessel undergoing maneuvers using four pairs of hydrophones, showing a directionality pattern with a frequency-independent broadside maximum, up to 12 dB greater than bow and stern levels. Horizontal noise directivity patterns have been developed [55] using a model to predict SL and spectral characteristics from ship length and geospatial (AIS) data, tested against empirical data collected in a shipping lane off South Korea. Discrepancies were attributed to ambient noise or a lack of reliability in the model chosen.

III. NORTHERN WATCH EXPERIMENT

DRDC operates an Arctic research camp at Gascoyne Inlet in the Barrow Strait, shown in Fig. 1, and in 2015 deployed a pair of 48-hydrophone HLAs referred to as the Arctic acoustic arrays (AAA1 and AAA2) as part of the Northern Watch experiment [56]. During the summer field season, the arrays have been activated for continuous operation for up to a month. This ice-free period coincides with the summer peak in ship traffic, primarily

comprised of cruise and cargo ships, government icebreakers, and pleasure craft [57] transiting through the Northwest Passage. Array data collected during August 2015 and 2019 were used in this study. Unlike merchant vessels typically seen in ocean transit lanes, the traffic near the Northern Watch site tends to be dynamic, with frequent changes in speed, heading, operating modes, and acoustic visibility as they navigate in and out of the nearby bays.

A. Acoustic Environment

Acoustic modeling in Barrow Strait is challenged by the complexity of the sea bottom properties [58]. Barrow Strait is a 60-km-wide channel with a maximum water depth of about 400 m. The sea bottom consists of various types of sediments, ranging from thin unconsolidated mud to thick glacial drift and glaciomarine deposits. A geoacoustic model based on previous studies [59] was used to represent the bottom layer as a single fluid with density, compressional speed, and compressional attenuation parameters that depend on the sediment type. The thickness of the bottom layer was assumed to vary linearly with water depth, from 5 m in shallow areas to 100 m in deep areas.

Two sound-speed profiles were collected at the locations noted by SSP1 and SSP2 in Fig. 1, and the profiles are shown in Fig. 2, with the corresponding RAMGeo acoustic propagation model results. For this study, the 2015 closest point of approach (CPA) of Ocean Endeavour was modeled using a range-dependent bathymetry and sound speed grid, for its tonal frequencies at 380, 505, and 545 Hz; results from the 505 Hz model at a CPA range of 1370 m to the 123-m deep hydrophone are presented in Fig. 2.

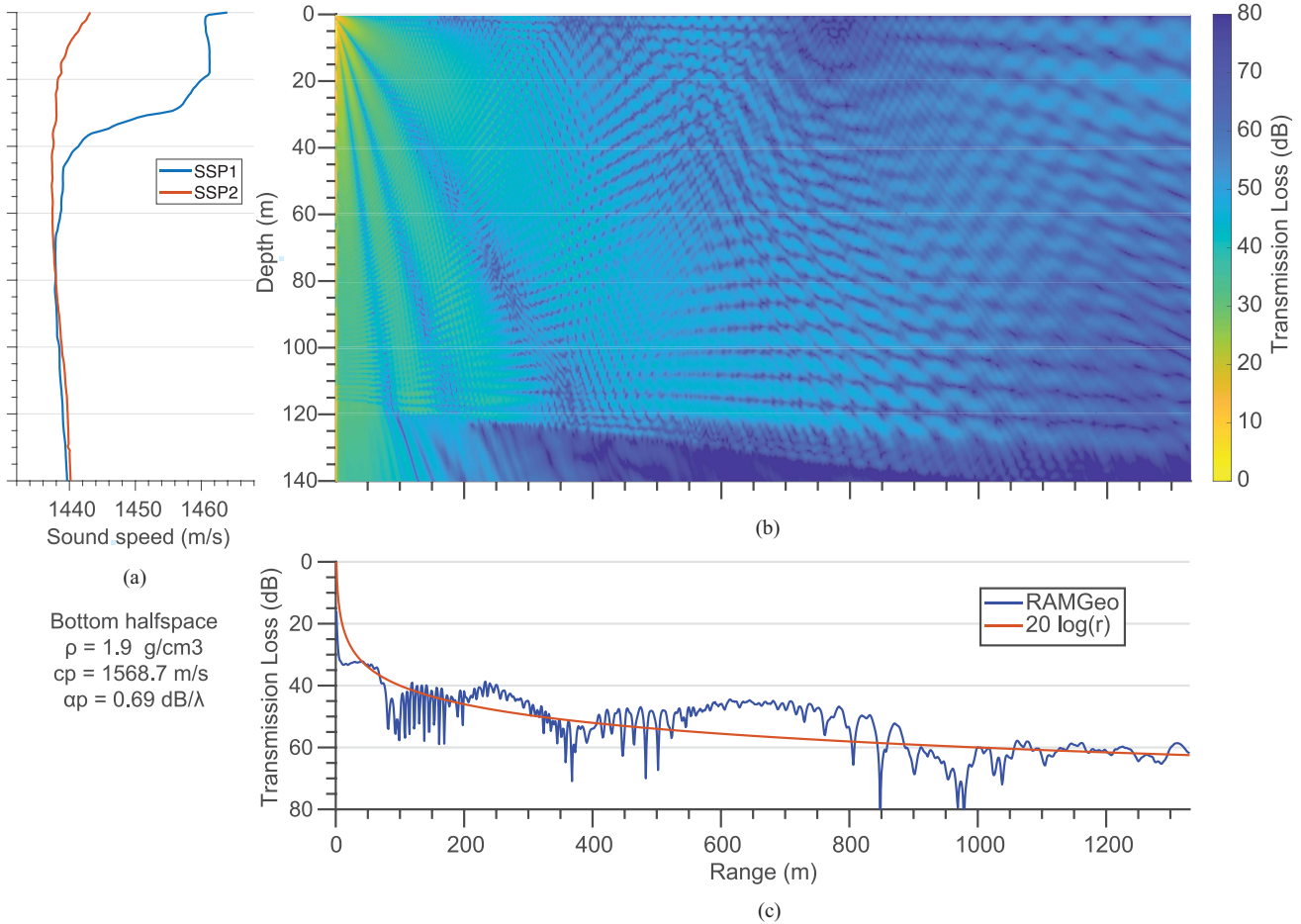


Fig. 2. (a) Sound-speed profiles taken in the region and used in the propagation loss (PL) modeling of the 505-Hz engine harmonic tonal over (b) range and depth and at (c) 130 m corresponding to the depth of AAA1, Hydrophone #24. The source, a dipole at 5.4 m depth, represents the Ocean Endeavour during its closest point of approach to AAA1 on 30 August 2015. The PL was computed using RAMGeo and the geoaoustic properties listed, with the geometric spreading loss shown for comparison (red).

B. Arctic Acoustic Arrays (AAA1/AAA2)

The HLAs were designed to form an aperture of 119 m (total length 150 m). Calibration of the 96 hydrophone elements that make up AAA1 and AAA2 was conducted in lab conditions before their deployment in 2015 and has not been repeated. The 150-m-long bottom-mounted, shore-cabled HLAs are deployed in 122–125 m and 176–177-m water depths, respectively, with a mainly flat response in the 100–600 Hz band. Some degradation of the hydrophones may be evident in the narrowband 1-Hz levels in Fig. 3, where three CPAs of the same ship in 2015 and 2019 are compared. Above 600 Hz, the arrays have an unexpected gain that was not apparent in 2015. Clipping in the 27 August 2019 recording resulted in an estimated SL of as much as 16 dB lower in 2019 than a CPA in 2015 under comparable speed and operating conditions. Clipping was observed in other acoustic records for some ships with very close-range CPAs; these records have been discarded from the results presented here.

IV. METHOD

SL directivity patterns are estimated based on the SL measurement concept described in American National Standards

Institute (ANSI) S12.64-2009 [33] adapted for the tonal components present in the unique signature of ships of opportunity, are produced using a signal processing method adapted from [1] and [53].

A. Ships of Opportunity

Acoustic pressure time series data were recorded continuously on AAA1 and AAA2 from 29 July to 30 August 2019. Time series data were preprocessed for spectral analysis and filtering: each ship pass in the 768 h of data was analyzed manually, characterizing unique contacts with

- 1) multiple passes with a CPA within 3 km of the array;
- 2) no secondary contacts within 10 km;
- 3) received levels (RL) greater than 10 dB above background levels.

Four ships were identified: Canadian Coast Guard Ship Des Groseilliers (DG), Cruise Ships Ocean Endeavour (OE), Roald Amundsen (RA), and The World (TW). The CPA parameters are in Table I, and spectrograms of the three OE CPAs (only the first two were used for SL estimation due to clipping in the third) are shown in Fig. 4.

TABLE I
CLOSEST POINTS OF APPROACH (CPA) FOR THE FOUR VESSELS OF OPPORTUNITY CHOSEN FOR THIS STUDY, INCLUDING CPA RANGES TO THE CENTER POINT OF AAA1 AND AAA2, SPEED AT CPA, AND THE VERTICAL ANGLE θ BETWEEN THE ARRAY AND THE SHIP AT CPA

Ship		CPA Time		Range [m]		Speed [m/s]		$\theta_{vertical}$ [°]	
ID		AAA1	AAA2	AAA1	AAA2	AAA1	AAA2	AAA1	AAA2
DG	Length (L): 98 m	8-18 9:11	8-18 9:29	2900	2170	4.6	4.3	3.0	2.8
DG	Draft (D): 7.4 m	8-29 11:30	8-29 11:00	2010	1830	3.2	3.0	3.7	2.4
OE	L : 137 m	8-30* 9:51	8-30* 9:51	1310	1750	5.9	6.1	8.5	14.0
OE	D : 5.8 m	8-05 4:18	8-05 4:08	1930	2670	6.0	6.0	3.9	2.8
RA	L : 134 m	8-28 11:24	8-28 11:42	1540	1080	4.0	4.0	3.7	5.7
RA	D : 16 m	8-28 23:30	8-28 23:20	2000	1570	6.9	7.4	23.4	2.7
RA		8-29 0:40	8-29 0:45	620	1700	8.1	7.3	33.0	2.5
TW	L : 196 m, D : 9.2 m	8-27 18:00	8-27 18:10	1575	430	7.1	4.4	4.1	23.4

All CPA times are from 2019 except OE 8-30 244 CPA, denoted by *, from 2015.

Two of the vessels, the DG and RA, use an electric prime mover, a two-step energy transfer system that first converts engine power to electrical current to power an electric motor that drives the propeller shafts, whereas the OE and TW utilize a diesel reduction system, where a direct mechanical coupling exists between the propeller shaft and the engine. DG is a light icebreaker, requiring the instantaneous torque available from the electric motor, with diesel engines providing the power generation. RA is a unique hybrid design combining a diesel generator with a bank of batteries that store power to enable short periods underway without the combustion engines running at all; the electric motors power the azimuth drive in an “L” configuration through a high-ratio bevel gear which allows the relatively small motor to operate at higher speed. Each of the four has 4-stroke primary engines with twin-screw propulsion. These ships are representative of the types typically encountered in the unique Arctic shipping environment, but not the global shipping fleet.

The world’s first hybrid cruise ship, RA, was recorded on the NW arrays as she made her 2019 maiden voyage across the northwest passage [60]. The four Bergen B33:45L6 diesel engines charge a 1356-kWh battery pack for surge power normally provided by running an additional engine. The reduced engine runtime provides an opportunity for fuel and emissions savings and should translate into a reduction in URN. This ship is propelled by twin vertical shaft permanent-magnet driven pulling thrusters with 4-bladed controllable-pitch propellers.

B. Signal Processing

Acoustic data were preprocessed by converting 10-min segments of a binary data format into a single HDF5 container with a time stamp and automatic gain level for each sample period, with a sample rate $f_s = 2500$ Hz. An automatic gain G_{AGC} was applied during the recording, dynamically stored

in the HDF5-formatted file, and subsequently removed during processing. The pressure time series

$$p_{in} = 2V_{fs} \cdot \frac{x_{float}}{2} \cdot 10^{-\left(S + G_{A/D} + G_{AGC}/20\right)} \mu Pa \quad (6)$$

was recorded with full-scale voltage, $V_{fs} = 5$ V, converted to +/-1 floating point x_{float} , and has a processing gain due to analog-to-digital conversion

$$\begin{aligned} G_{A/D} &= 20 \log_{10} (P_{out}/P_{in}) = 20 \log_{10} (2/5) \\ &= -7.96 \text{ dB re } \frac{1 \mu Pa}{V}. \end{aligned} \quad (7)$$

Clipping was observed in some cases when the amplitude of the acoustic signal exceeded the dynamic range of the recording system, typically during a close-range CPA. To ensure the integrity of the SL estimates, all instances of clipping observed were manually identified and excluded from the analysis.

1) *Received Level Spectrum:* To calculate the underwater SL spectra from the archival data, each of the 48 channels of recorded pressure time series with $f_s = 2500$ Hz were divided into consecutive, nonoverlapping data segments of length $T_s = 3$ s. For each segment, the acoustic time series were processed using a two-sided fast Fourier transform (FFT) of size N_{FFT} with a rectangular window and 60% overlap. The resulting mean pressure squared values for frequencies in bins of width $BW = f_s/N_{FFT}$ received a hydrophone-specific calibration correction and were converted to received sound spectrum levels in dB referenced to $1 \mu Pa^2/Hz$. The FFT processing gain was offset with a factor of $2/N_{FFT}^2$ and FFT coefficients are smoothed using a five-segment (15 s) unweighted moving average. For broadband processing, $N_{FFT} = 2500$, and the resulting time-frequency distribution $|\overline{FFT}|^2$, known as a spectrogram, contained the squared received sound pressure levels (RLs) in 1-Hz bins for each hydrophone, which were reported in dB

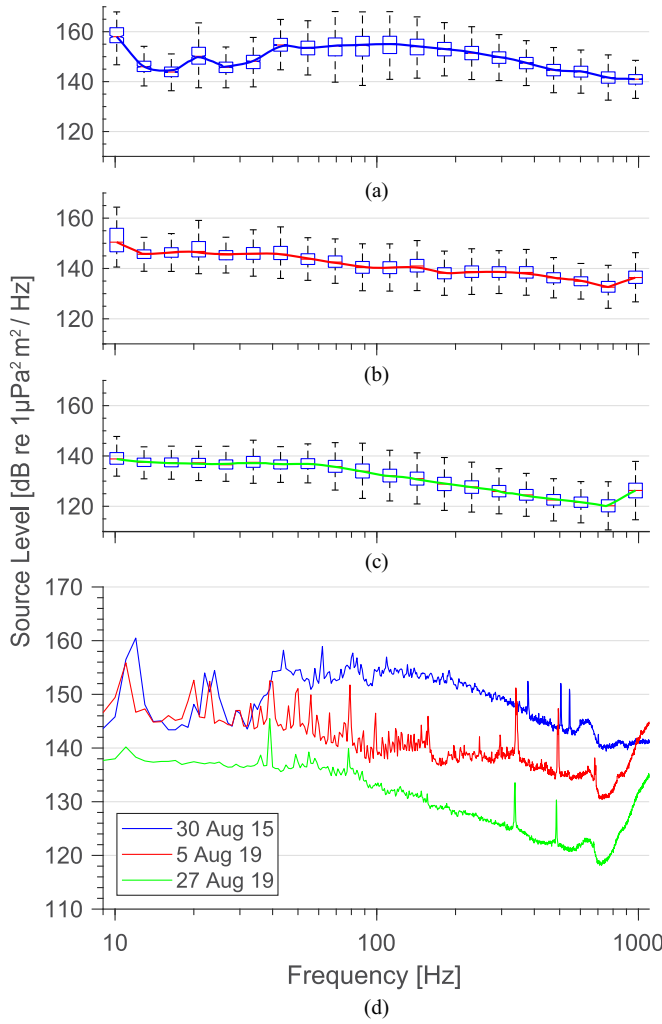


Fig. 3. Source level box plots in 1/3 octave bands for the 48 hydrophones in AAA2 computed over 65 min centered on the Ocean Endeavour's closest point of approach on (a) 30 August 2015, (b) 5 August 2019, and (c) 27 August 2019 (discarded from results for clipping). (d) 1-Hz resolution mean computed over the same window for the same three passes, showing the prominent tonals at 379, 505, and 545 in the midfrequency band.

referenced to $1 \mu\text{Pa}^2$

$$\text{RL} = 10 \log_{10} \frac{|\text{FFT}|^2}{(1 \mu\text{Pa})^2}. \quad (8)$$

2) *Spectral Analysis:* Spectral analysis of the ships' signature requires measuring the periodic engine (CFR) and propulsion (SR and BR) frequencies. Auxiliary, mechanical, electrical, and hydrodynamic noise sources were identified based on the spectral characteristics and relative frequency dynamics described in Section II. Ship specifications such as engine, gearbox, thruster, and propeller types, maintenance activities, and operating characteristics were collected to aid in attribution. Once the source dependence of the ship signature is known, tonal components can be grouped by type. An example of this method is presented in Section V.

3) *Bandpass Sampling:* The 1-Hz bins derived for RL estimation were well-suited to the measurement of URN levels but lacked the frequency resolution necessary for the identification and tracking of tonal frequency components and their harmonics, where time-frequency distributions with frequency resolutions on the order of 0.1 Hz are appropriate. To achieve this resolution acoustic data were reprocessed with $N_{\text{FFT}} = 25\,000$ to produce spectrograms with fine frequency resolution, but insufficient time resolution for frequency tracking of dynamic tonals. A bandpass sampling approach was used [61], which provided sufficient frequency resolution for spectral analysis while maintaining appropriate time resolution to identify frequency shifts and instabilities. Time-series data were subsampled in time blocks, then filtered across the frequency band $[f_1, f_2]$ of bandwidth $B = f_2 - f_1$ using a complex one-sided bandpass filter centered on

$$f_c = (f_1 + f_2)/2 \quad (9)$$

to then downsample the time series by f_s/B , which brought $[f_1, f_2]$ to the baseband $[0, B]$, and a 2500-point FFT then provided the desired 0.1-Hz frequency resolution.

4) *Tracking Tonals With Dynamic Frequencies:* Tonal sources such as engine CFR harmonics and gear mesh rates can be modulated in both frequency and amplitude. Amplitude shifts occur due to random fluctuations of mechanical vibrations, whereas machinery speed changes lead to nominal frequency shifts; relative frequency shifts are due to the Doppler effect observed at the receiver during ship maneuvers or at CPA. To estimate the URN attributable to a discrete tonal source whose center frequency and bandwidth vary in time, frequency-domain tracking of the signal is employed. The frequency tracking algorithm, for each time segment, is given as follows:

- 1) apply the bandpass sampling method described in Section IV-B3 across a frequency subband five times the width of the measured frequency range $f_{\text{max}} - f_{\text{min}}$ of the tonal;
- 2) calculate the RL spectra as described in Section IV-B1 for this subband;
- 3) a sliding time window compares RL across the frequency subband to find the local maxima and returns RL and center frequency;
- 4) a moving average of frequency bins filters maxima that have drifted too far from the mean to smooth the frequency track;
- 5) adaptive thresholding is used to track the signal through noisy periods.

The algorithm returns the narrowband RL estimates, center frequency, and prominence for each tonal source.

C. Automatic Identification System (AIS)

AIS data were collected using both a ground-based AIS system located at the Gascoyne Inlet camp, as well as satellite AIS tracks obtained through *ExactEarth*. The disparate data sets were combined and smoothed using a moving average filter,

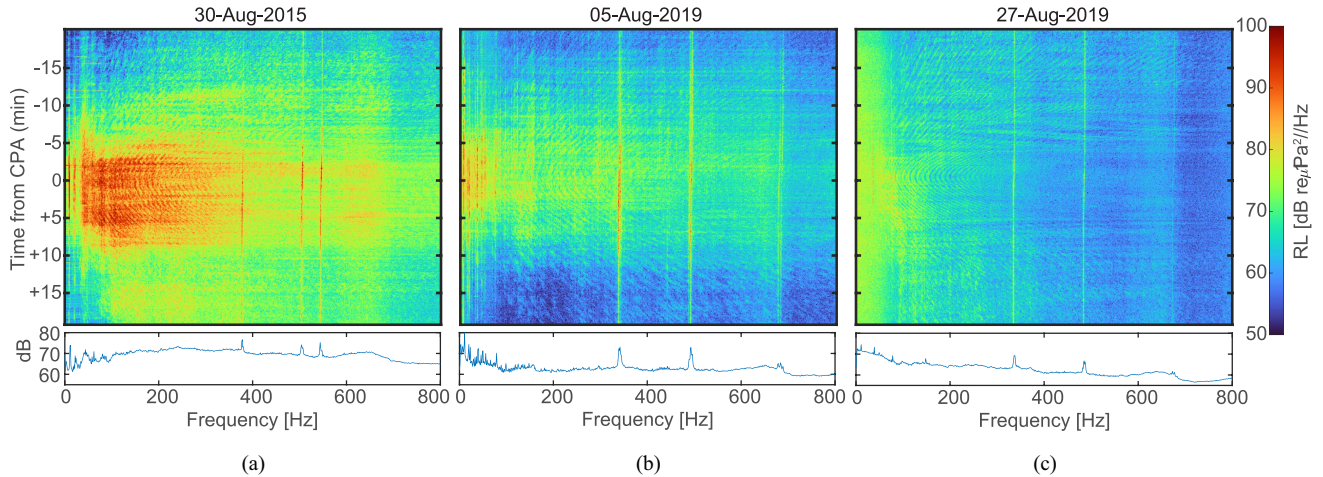


Fig. 4. 1-h, 0–800 Hz, 1024-point (a) mean spectrum and (b) Hamming window spectrogram of Ocean Endeavour passing AAA1 on 5 August 2019 at a speed of 6.2 m/s (12 kn), with two prominent tonal components evident at 340 and 497 Hz.

to provide a continuous time series of locations, course over ground, and speed estimates for each contact during the period of interest. The discrete AIS transmission instants were aligned with the acoustic data segments using a linear interpolation along the ship track, but some clock error was introduced from the lack of synchronization between the two systems. The coordinates transmitted over AIS typically represent a location on the bridge that does not correspond to the acoustic center of the ship. This may introduce a positioning error of up to ~ 10 m between the AIS location and the assumed noise source location.

Slant range R was calculated from ship to receiver for each hydrophone h at each time step i and used to calculate PL such that

$$R_{ih} = \sqrt{(d_h - d_s)^2 + r_{ih}^2} \quad (10)$$

where d_h is the depth of hydrophone h , d_s is the draft of the ship minus estimated propeller diameter, and r_{ih} is the lateral range from the ship's AIS transponder to hydrophone h at time step i .

Aspect angle was calculated by taking the difference of the incident angle between ship and hydrophone, and the ship heading as reported in the AIS transmission. The angular distribution of the ship's URN is thus determined by sorting events according to aspect. To avoid contamination of the acoustic signature data, events where a secondary AIS contact was within 10 km of either array were discarded.

D. SL Estimates

SL was estimated from RL and R using a geometric spreading model. A numerical modeling study was conducted [62] using RAMGeo, a range-dependent parabolic equation model, to assess the validity of the geometric spreading assumption and provide a suitable local spreading constant for the geometric PL model. CTD casts were conducted at two proximate locations shown in Fig. 1, during a calm August day. The shallower, near-shore location showed warmer surface waters and a stronger downward-refracting character than the deeper, well-mixed waters toward the channel. For the 0–1000 Hz frequency band

and the shallow (<200 m), slightly downward-refracting polar environment modeled, a suitable fit could be provided using a geometric spreading model based on the slant range R defined as the distance from the midpoint of the ship to the receiver

$$\text{SL} = \text{RL} + 20 \log R. \quad (11)$$

Modeling results showed acceptable agreement between the inverse square model and the PL estimated by RAMGeo at most ranges; as shown in Fig. 2, the environment is supportive of strong multipath interference, particularly on calmer days when muted surface roughness induces less scattering. The inverse square model may be inadequate at these interference minima, where the two models displayed as much as 20 dB of disagreement in the first 1 km.

E. SL Probability Densities

SL was estimated for both broadband and discrete tonal sources for each time segment in the ~ 1 h CPA events of the four vessels. Empirical probability densities were calculated for the ensemble of SL estimates, grouped according to aspect angle and visualized in a 2-D polar coordinate system with (0,0) representing the acoustic center of the ship, 0° the ship's bow aspect, and 180° the stern, 90° the starboard beam, and 270° the port beam. The radial distance from (0,0) corresponds to the URN level, with the density of samples measured at that level corresponding to the empirical probability density color bar next to each figure. These polar densities represent the relative likelihood of observing a nominal SL as a function of aspect angle, which has been referred to here as URN directivity patterns.

V. RESULTS

The approach described in the preceding section was carried out for each of the CPA events in Table I at each of the 48 hydrophones in 2 arrays, providing 96 samples per ~ 1 h CPA event. This section presents the spectral analysis and SL estimates from three CPA events for OE and RA.

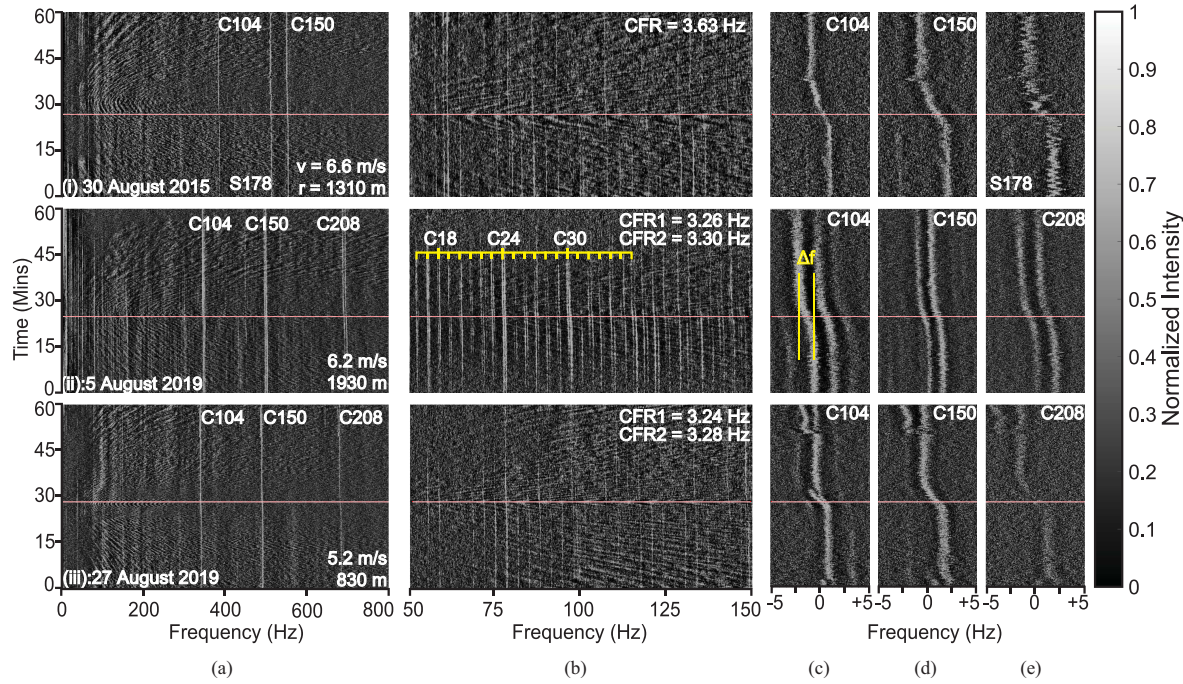


Fig. 5. 1-h spectrograms of Ocean Endeavour passing AAA1 on (i) 30 August 2015, (ii) 5 August 2019, and (iii) 27 August 2019, showing the broadband (a: 0–800 Hz), engine band (b: 50–150 Hz), and individual narrowband tonals (c, d, and e: 10-Hz window over the tonal center frequency, shown in white). The speed and closest point of approach distance are given in (a.i–iii), whereas the cylinder firing rates (CFR) are given in (b.i–iii) and illustrated across harmonics C16–C36 with the yellow dividers (b.ii). The red line shows the closest point of approach for the three passes, and the yellow spacing in (c.ii) corresponds to the Doppler shift Δf .

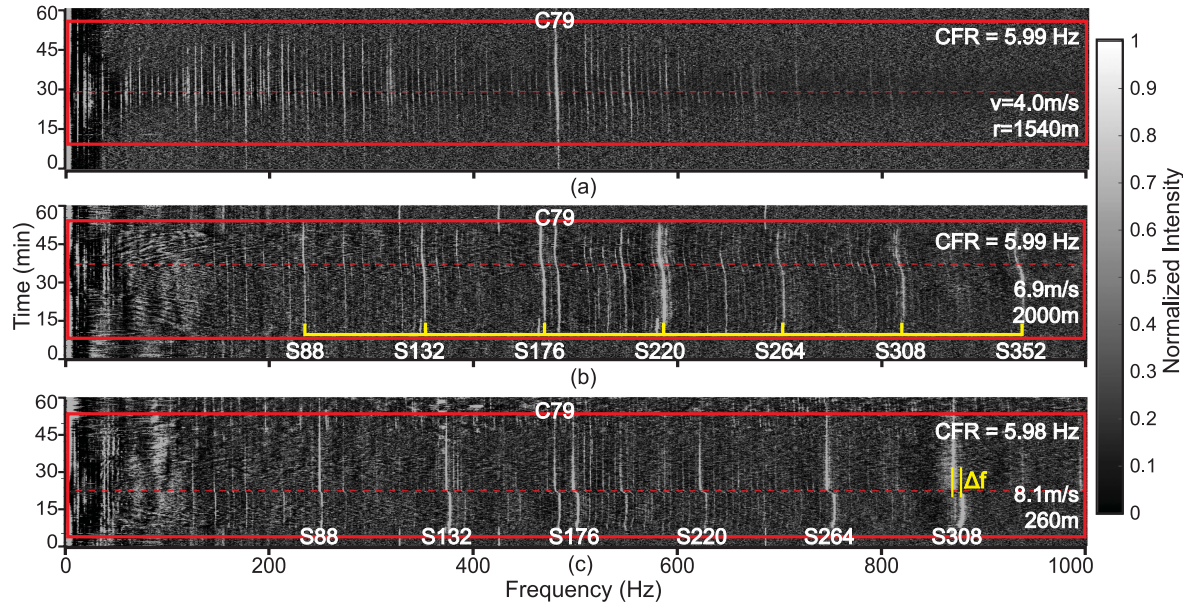


Fig. 6. 0–1000 Hz spectrograms for Roald Amundsen during (a) 28 August (b) 28 and 29 August, and (c) 29 August 2019, each with 2.5-h durations. The red box indicates the 1-h analysis period around the closest point of approach (red dashed line) of the three passes. The vessel speed is indicated in the top left of each red box, the primary cylinder firing rate in the top right, and the predominant tonals are labeled.

A. Diesel Reduction Spectrum

OE was chosen as a representative example due to its relatively simple acoustic signature, owing to its conventional diesel reduction configuration, with harmonic tonal components related

to both the engine and propulsion and stable tonal sources. Three viable OE CPAs were identified, with parameters in Table I, for 1) 30 August 2015, 2) 5 August 2019, and 3) 27 August 2019; however, SL estimates from 3) are excluded due to hydrophone clipping.

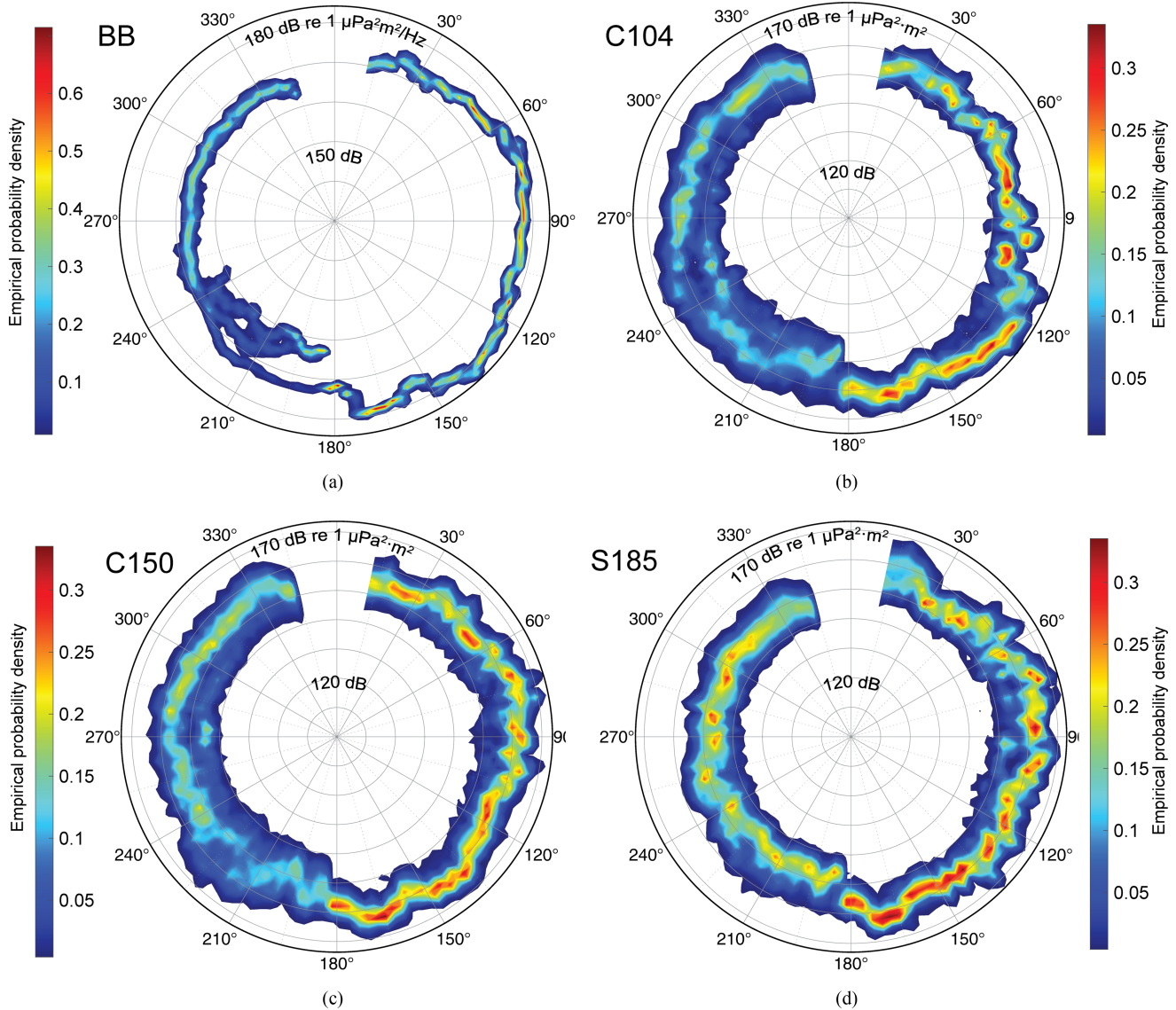


Fig. 7. Source level (SL) probability densities as a function of Ocean Endeavour ship aspect for (a) broadband (100–600 Hz), (b) C104 (104 times the cylinder firing rate, CFR), (c) C150 (150 × CFR), and S185 (105 × propeller shaft rate). SL was estimated from received pressure levels from two passes of the ship over both hydrophone arrays and correcting for propagation loss with an inverse square model. AIS positioning and heading data were used to obtain continuous distance and aspect angle to each array element; 0° represents the bow aspect of the ship. Tonals at C104 and C150 were present for all passes; the tonal at S185 was observed only during the 2015 detection of Ocean Endeavour.

Tonal components were identified starting in the 0–800-Hz spectrograms in Fig. 5(a.i-iii), using a 2048-point FFT producing 0.5-Hz frequency resolution. This wideband analysis display shows a Lloyd's mirror interference pattern, caused by the constructive and destructive interference of multipath propagation. The interference pattern converged to a minima visible in each of Fig. 5(a.i-iii) and (b.i-iii) corresponding to the CPA time shown as a red line in each frame. The wideband spectrogram was also used for identifying prominent tonals for each CPA: 104 × CFR, referred to as C104 and inspected in detail in Fig. 5(c.i-iii); C150 in Fig. 5(d.i-iii); C208, or the second harmonic of C104, detected on events (i) and (ii) only and highlighted in Fig. 5(e.ii-iii); and 178 × SR or S178, detected on (i) only and inspected in Fig. 5(e.i). A 15.6-Hz analysis band was applied over each of the three sets of tonals using a 2048-point

FFT to produce 0.038 Hz frequency bins. This fine resolution permits detailed analysis, including identifying the number of engines operating, signal bandwidth and stability characteristics, and Doppler calculations.

Fig. 5(b.i-iii) shows the 50–150 Hz band where diesel engine noise is predominant. The spectrogram identifies a tonal signature dominated in this midfrequency band by the first ~60 harmonics of the CFR of two engines, in this case, 3.26 and 3.30 Hz, shown with the yellow harmonic dividers in Fig. 5(b.ii) with spacing equal to CFR1.

The diffusive nature of the tonal in Fig. 5(e.i), with high-frequency oscillation of the center frequency, was indicative of a reduction gear mesh rate. Instability was apparent here compared to the more stable predominant CFR harmonics. The acoustic signature for OE showed a notable change between the 2015 and

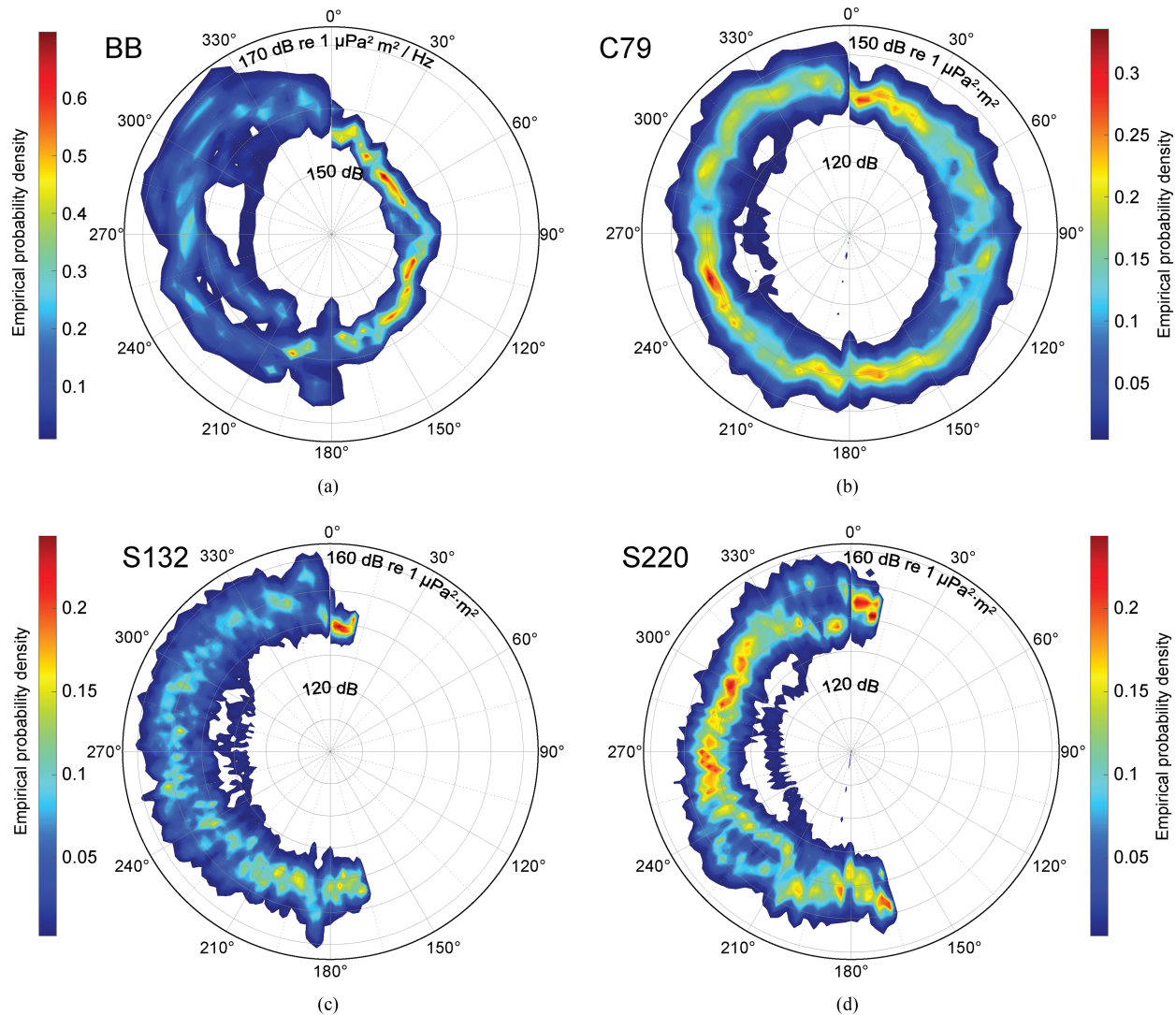


Fig. 8. Source level (SL) probability densities as a function of Roald Amundsen ship aspect for (a) broadband (100–600 Hz), (b) C79 (79 times the cylinder firing rate, CFR), (c) S132 (132 \times propeller shaft rate, SR), and (d) S220. SL was estimated from received pressure levels from 3 unique passes of the ship over both hydrophone arrays and correcting for propagation loss with an inverse square model. AIS positioning and heading data were used to estimate continuous distance and aspect angle to each array element; 0° represents the bow aspect of the ship. The tonal at C79 was present for all three passes; the tonals at S132 and S220 were observed only during the two high-speed passes.

2019 events, visible in the acoustic spectrum where the shaft-related source [S178 in Fig. 5(e.i)], possibly attributable to a reduction gearset, was no longer present following maintenance conducted in 2016 and 2018.

B. Diesel-Electric Hybrid Spectrum

RA made three passes of the arrays between 10:00 on 28th August and 01:00 on 29th August, with a notable difference in the acoustic signature observed at 4 m/s [see Fig. 6(a)] and 7–8 m/s [see Fig. 6(b) and (c)]. Four, 4-stroke engine signatures with constant CFRs of 5.97–6.01 Hz were apparent for this diesel-electric hybrid configuration. All CPAs showed an engine-driven source at 79 times the CFR (C79) at 475.4 Hz. The high-speed passes showed a more pronounced Lloyd's mirror at CPA, but most significantly a tonal source emerged at 44 times the propeller shaft rate (115.4 and 122.8 Hz), with harmonics 1–8

predominant. Shaft-rate banding ($SR = 2.61$ Hz and 2.86 Hz) was evident around the tonals suggesting a coupling to the propeller shaft, with a rotation 44 times the shaft rate (S44). These pulling thrusters drive the propeller and draw power through a vertical input shaft connected to the permanent magnet electric motor. Because the electric motor does not require a reduction gearing as in a diesel reduction configuration, the frequency relationship between this source and the shaft rate suggests the S44 is the frequency of rotation of the AC motor within this azimuth thruster.

C. Frequency Shifts

Examples of the frequency shift due to Doppler are shown in yellow in Figs. 5(c.ii) and 6(c). Equation (4) was used to estimate the contact speed, which is reduced to (5), as $\theta = [0^\circ, 180^\circ]$ was assumed based on the long detection period and close-range

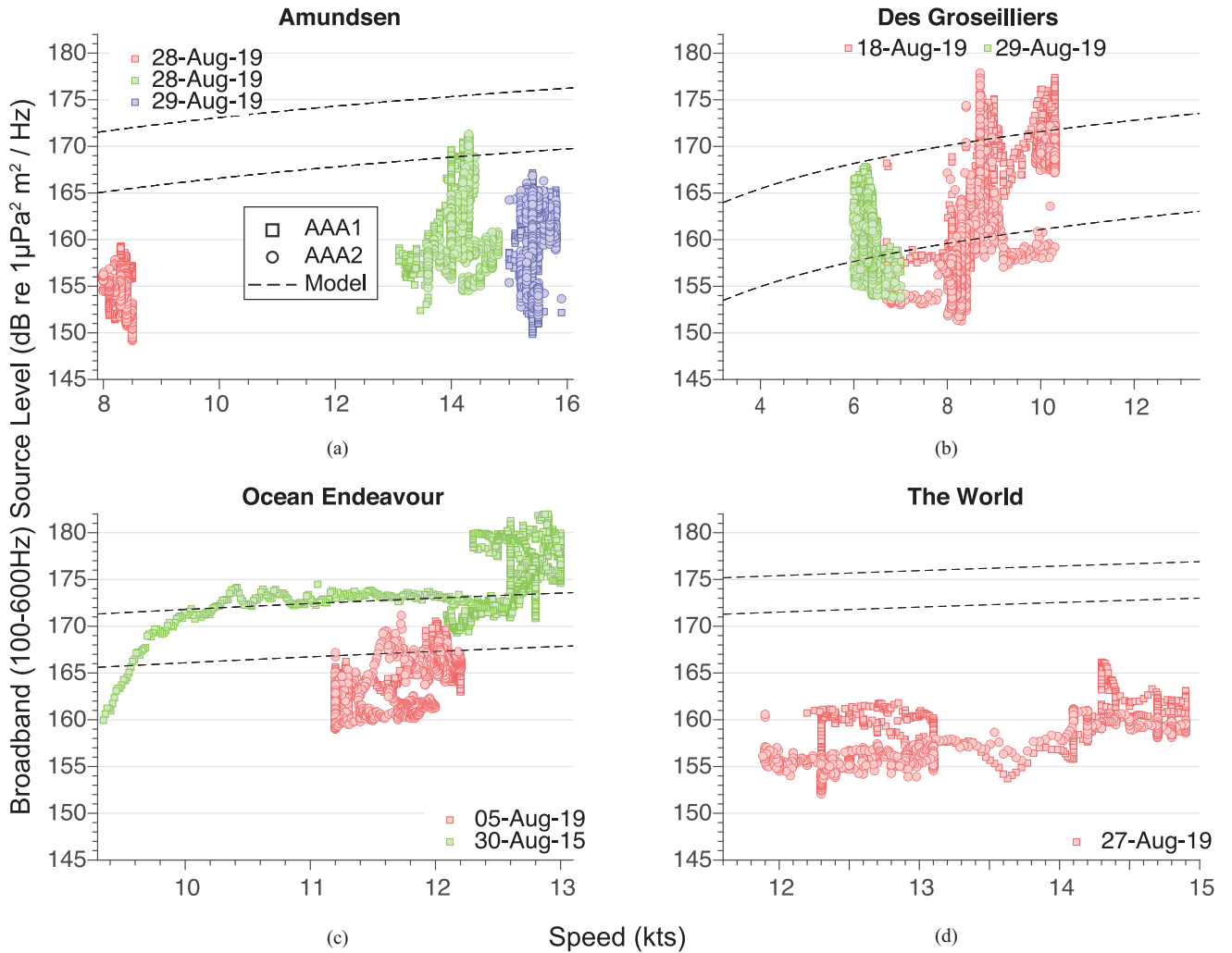


Fig. 9. Broadband source level estimates over AIS speed for four ships of opportunity with 2–4 CPAs each: Colors distinguish different CPA events as noted in the legends. Circle markers indicate array 1 and square markers indicate array 2.

CPA. The analysis bands in Fig. 5(c)–(e) show Doppler shifts in C150 of $\Delta f = 4.4$, 3.9, and 3.4 Hz, for center frequencies $f_c = 545.7$, 494.5, and 486.0 Hz. Solving (5) for v with $\bar{c} = 1441$ m/s provides Doppler speeds of 6.0, 5.8, and 5.2 m/s. These are in close agreement with the AIS data shown in Fig. 1 with CPA speeds of 5.9, 6.0, and 5.2 m/s.

Using a 25 Hz frequency band centered on the tonal center frequency, the tracker was able to identify a discrete tonal center frequency and estimate signal bandwidth and prominence for each time segment with an error rate proportional to the signal-to-noise ratio of the source. Frequency shifts were detected without any notable lag, limited only by the resolution of the time window. The tracker performance deteriorates for tonals with 1) low signal-to-noise ratios and 2) high instabilities, where the error rate rapidly increases signal tracking is lost.

D. Radiated Noise

SL characteristics differed significantly between ships, and in some cases among different observations of the same ship, when engine speeds or operating parameters were changed, or

propeller cavitation was induced. The SL directivity patterns are shown as empirical probability densities. Midfrequency (100–600 Hz) tonals were selected for these comparisons to optimize for the band of peak hydrophone sensitivity. Cavitation is not measured directly but influences SL most significantly above a ship's CIS.

1) *Ocean Endeavour*: Radiation patterns for 100–600 Hz broadband and three tonal sources shown in Fig. 5 were computed and presented in Fig. 7. The broadband radiation pattern in Fig. 7(a) shows a tight distribution of SL estimates that is multimodal on the starboard aspect. The peak broadband SL was found on the starboard side at 182 dB re $1 \mu\text{Pa}^2 \text{m}^{-2}$, whereas the SL at the bow aspect was estimated to be 10 dB lower. The port aspect has a tight distribution of SL between 240° and 345° , where the mean SL is 168 dB re $1 \mu\text{Pa}^2 \text{m}^{-2}$. The cluster of wider SL distribution and broadband SL minima between the stern aspect and 240° coincides with a speed decrease and maneuvering as OE sailed away from the arrays on 30 August 2019.

Fig. 7(b) for C104 shows a small peak in SL of 172 dB re $1 \mu\text{Pa}^2 \text{m}^{-2}$ on the starboard side of the port aspect at 130° and a

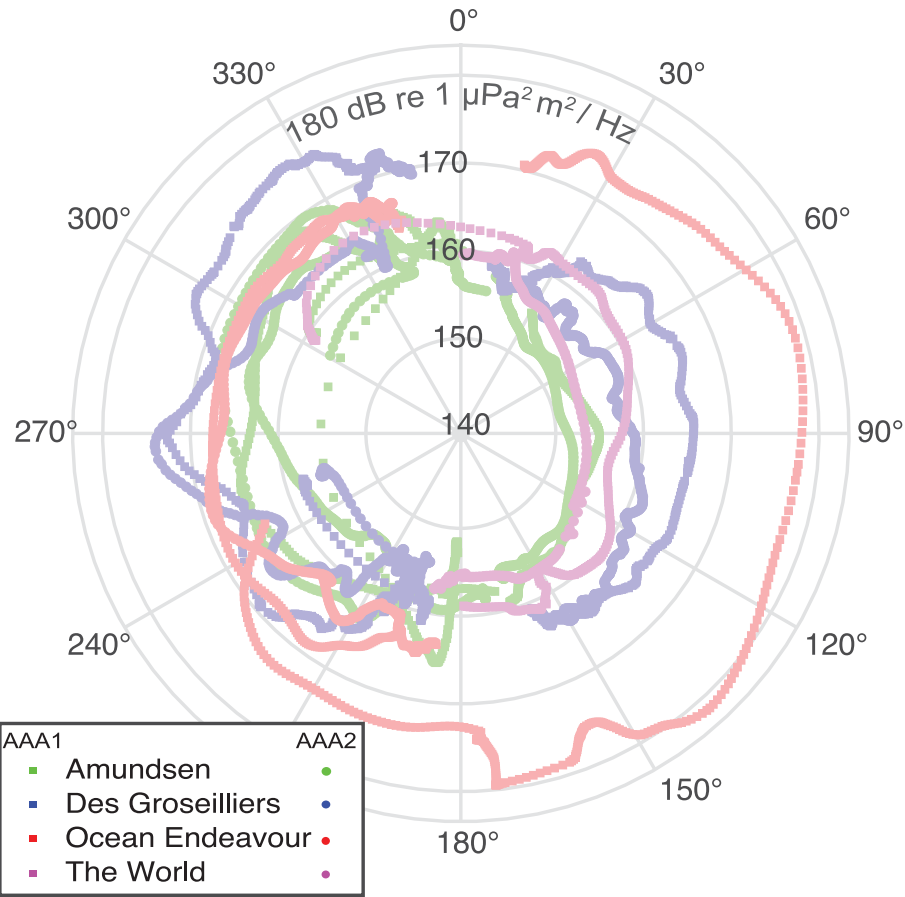


Fig. 10. Broadband (100–600 Hz) source level estimates as a function of ship speed for (a) Amundsen, (b) Des Groseilliers, (c) Ocean Endeavour, and (d) The World.

roughly omnidirectional profile and has a similar distribution to the other CFR harmonic C150 in Fig. 7(c). The minima for these engine-related sources were seen during the starboard CPAs. The shaft-related tonal S185 in Fig. 7(d) has a bias toward higher SL on the stern aspect. No significant distinction was noted between radiation patterns for engine-related tonals (C104, C150) and shaft-related tonal (S185).

2) *Roald Amundsen*: Radiation patterns for 100–600-Hz broadband and three tonal sources shown in Fig. 6 were computed and presented in Fig. 8. The broadband radiation pattern in Fig. 8(a) shows a narrow spread of SL on the starboard aspect with means of 152–157 dB re $1 \mu\text{Pa}^2 \text{m}^2$ and a wider spread of SL on the port aspect. This was an artifact due to the starboard aspect containing SL measurements taken from a single pass, as shown in Fig. 6(c), where the CPA on AAA1 was at an extremely close range (200 m). At this range, the PL model performed poorly, as predicted by the model comparison in Fig. 2, which suggested PL could be underestimated by as much as 20 dB over short ranges coinciding with interference minima. On the port aspect, a broader range of SL was measured from two CPAs shown in Fig. 6(a) and (b), with ~5 dB greater SL measured on the beam than the stern aspect.

The CFR-related tonal C79 in Fig. 8(b) showed a roughly omnidirectional SL profile, with a mean ranging from 139 dB re

$1 \mu\text{Pa}^2 \text{m}^2$ on the starboard bow aspect to 145 dB re $1 \mu\text{Pa}^2 \text{m}^2$ on the port bow aspects. The shaft-related tonals S132 in Fig. 8(c) and S220 in Fig. 8(d) were detected only on the two high-speed CPAs in Fig. 6(b) and (c) when the RA passed the arrays on the port aspect. S132 showed ~7 dB higher SL on the bow aspect than the stern.

3) *Comparison Across Platforms*: Broadband SL was compared to instantaneous vessel speed from AIS in Fig. 9. For individual vessels, a positive correlation was observed where increasing vessel speed is indicative of greater SL, with good agreement with the vessel speed term in the Chion model. The correlation was biased lower due to SL measurements at close range where the PL model performs poorly. SL measurements were compared to the broadband SL model which appears as dashed lines in Fig. 9(a)–(d). The two dotted lines represent the Chion model's predictions with a distance correction term of $-4.83 \log [\text{range}/1 \text{ nm}]$ applied at the closest (CPA) and furthest (maximum SL range) distances. Both the RA and TW showed broadband SL 10–15 dB lower than predicted by this model, suggesting these ships are quiet for their classes. SL measurements for DG and OE were concentrated near the levels predicted by the model.

The polar plot in Fig. 10 compares broadband SL for individual CPAs of all vessels. OE shows the greatest range of variability

across its estimated SL, with a near 20 dB difference between minima and maxima at the beam aspect, with a maximum SL observed off the starboard stern aspect (140°). Greater broadband SL was measured on the stern aspect for all observations of this vessel, indicative of the strong influence of propeller cavitation in the vessel signature at the speeds observed.

DG's broadband signature showed strong variance between aspects, but a relatively tight spread between different CPAs. This was due to the high degree of signature variance for the ac/dc diesel-electric propulsion, which exhibited frequent and sudden speed changes. SL measurements were influenced by this unique configuration, where the dc electric motor is connected directly to its propeller, and the motor signature dominates the sound spectrum during speed changes, causing brief spikes in broadband SL.

TW offered port aspects at steady speeds and close-range CPAs of both arrays, suggesting low variance SL measurements, but the diesel-reduction engine operated dynamically, causing frequency shifts in the engine and propulsion-related tonals. The maximum observed broadband SL was $166 \text{ dB re } 1 \mu\text{Pa}^2 \text{ m}^2$.

RA had the lowest average SL and among the lowest SL at any aspect, with a maximum of $171 \text{ dB re } 1 \mu\text{Pa}^2 \text{ m}^2$ observed on the port bow aspect. The distribution of estimates was calculated for each 4° bearing bin with a mean standard deviation across all tonals of $\sigma_{NB} = 6.8 \text{ dB}$, and for broadband $\sigma_{BB} = 3.0 \text{ dB}$.

VI. CONCLUSION

Established ship noise measurement standards are well-suited for repeatability, but coarse octave sizing and long time averaging periods do not provide sufficient granularity to deliver insights about the horizontal directionality of noise components or interdependence between tonal components. An approach to estimate a horizontal directivity pattern for tonal and broadband sound pressure level measurements from a passing ship was described. Acoustic data from HLA and AIS ship tracks were analyzed using this method with empirical SL probabilities densities presented as a function of ship aspect.

Two cruise ships, one a diesel-electric hybrid (RA) and the other a diesel reduction configuration (OE), were compared in a case study. The diesel reduction showed many engine harmonics in its signature and a directionality profile that suggests greater noise lobing of engine-related components on the beams, whereas broadband noise has more omnidirectional components. While cavitation noise was not the focus of the analysis presented here, RA showed only weak cavitation at high speeds, likely owing to the homogenous inflow and reduced oscillations in shaft torque credited to the electric drive azipull thruster, and this noise efficiency was evident in the relatively low broadband and tonal SL at high speed when compared to other vessels.

Local bathymetry played an important role in SL estimation; the shallower water to the north of the arrays was associated with higher levels of variability between estimates, and measurements taken while a ship was traveling through this relatively shallow ($\sim 50 \text{ m}$) water tended to reflect higher SL estimates than when the same ship was observed in the deeper water to the south.

Nonstationarity of frequency tonals due to Doppler and the idiosyncrasies of different marine propulsion configurations presents challenges to automation in classification. A frequency tracking approach was described for calculating true tonal SLs, as the center frequency for tonal sources shifted due to the mechanical and operating conditions on the ship, and the Doppler shift seen at CPA.

Broadband SL was estimated between 148 and 181 dB re $1 \mu\text{Pa}^2 \text{ m}^2$ for the four ships of opportunity, and levels increased with vessel speed. Estimates were found to be generally in agreement or lower than the predicted levels in the Chion model. The quietest ship among the four was RA, with a maximum of $171 \text{ dB re } 1 \mu\text{Pa}^2 \text{ m}^2$ observed on the port bow aspect. Tonal levels ranged from 121 to 172 dB across all ships and aspects, and the distribution was wider for tonal components ($\sigma = 6.8 \text{ dB}$) than broadband ($\sigma = 3.0 \text{ dB}$). Propulsion-related tonals tended to have higher SL than engine-related tonals, whereas higher frequencies were associated with lower SL estimates.

At close ranges, the method performed poorly, with the geometric spreading model underestimating a numerical PL model by up to 20 dB, and SL was consequently biased lower for close-range CPAs and higher at longer ranges. The selection of the scaling factor for the spherical spreading model has an important effect on the resulting directionality estimates. Improvements to this method could integrate PL modeling for SL estimation, particularly for close ranges and for ships in shallower water where SL estimates were challenged. An assumed degradation in hydrophone sensitivity between calibration for the 2015 deployment and measurements in 2019 may introduce a tendency to underestimate absolute vessel SL.

ACKNOWLEDGMENT

The authors would like to thank the Canadian Department of National Defence using data collected by Defence Research and Development Canada and Dr. Garry Heard for dedicating his career to Arctic acoustic experimentation so that others could follow. Assistance with the method was provided by Dr. Martin Gassman. Perplexity.ai was used for proofreading.

REFERENCES

- [1] M. F. McKenna, D. Ross, S. M. Wiggins, and J. A. Hildebrand, "Underwater radiated noise from modern commercial ships," *J. Acoust. Soc. Amer.*, vol. 131, no. 1, pp. 92–103, 2012, doi: [10.1121/1.3664100](https://doi.org/10.1121/1.3664100).
- [2] C. Erbe, S. A. Marley, R. P. Schoeman, J. N. Smith, L. E. Trigg, and C. B. Embling, "The effects of ship noise on marine mammals—A review," *Front. Mar. Sci.*, vol. 6, 2019, Art. no. 606, doi: [10.3389/fmars.2019.00606](https://doi.org/10.3389/fmars.2019.00606).
- [3] C. M. Duarte et al., "The soundscape of the Anthropocene ocean," *Science*, vol. 371, no. 6529, 2021, Art. no. eaba4658, doi: [10.1126/science.aba4658](https://doi.org/10.1126/science.aba4658).
- [4] L. Bittencourt, M. Barbosa, T. L. Bisi, J. Lailson-Brito, and A. F. Azevedo, "Anthropogenic noise influences on marine soundscape variability across coastal areas," *Mar. Pollut. Bull.*, vol. 160, 2020, Art. no. 111648, doi: [10.1016/j.marpolbul.2020.111648](https://doi.org/10.1016/j.marpolbul.2020.111648).
- [5] R. L. Putland, C. A. F. de Jong, B. Binnerts, A. Farcas, and N. D. Merchant, "Multi-site validation of shipping noise maps using field measurements," *Mar. Pollut. Bull.*, vol. 179, 2022, Art. no. 113733, doi: [10.1016/j.marpolbul.2022.113733](https://doi.org/10.1016/j.marpolbul.2022.113733).
- [6] P. F. Worcester, "Ocean acoustics in the rapidly changing Arctic," *Acoust. Today*, vol. 16, no. 1, 2020, Art. no. 55, doi: [10.1121/at.2020.16.1.55](https://doi.org/10.1121/at.2020.16.1.55).
- [7] M. Ladegaard et al., "Soundscape and ambient noise levels of the Arctic waters around Greenland," *Sci. Rep.*, vol. 11, no. 1, pp. 1–15, 2021, doi: [10.1038/s41598-021-02255-6](https://doi.org/10.1038/s41598-021-02255-6).

- [8] G. Heard and S. Pecknold, "An Arctic environment baseline," DRDC-RDDC-2016-L280, 2016.
- [9] R. M. Rolland et al., "Evidence that ship noise increases stress in right whales," *Proc. Roy. Soc. B, Biol. Sci.*, vol. 279, no. 1737, pp. 2363–2368, 2012, doi: [10.1098/rspb.2011.2429](https://doi.org/10.1098/rspb.2011.2429).
- [10] W. D. Halliday, S. J. Insley, R. C. Hilliard, T. de Jong, and M. K. Pine, "Potential impacts of shipping noise on marine mammals in the western Canadian Arctic," *Mar. Pollut. Bull.*, vol. 123, no. 1/2, pp. 73–82, 2017, doi: [10.1016/j.marpolbul.2017.09.027](https://doi.org/10.1016/j.marpolbul.2017.09.027).
- [11] R. Williams, E. Ashe, L. Blight, M. Jasny, and L. Nowlan, "Marine mammals and ocean noise: Future directions and information needs with respect to science, policy and law in Canada," *Mar. Pollut. Bull.*, vol. 86, no. 1/2, pp. 29–38, 2014, doi: [10.1016/j.marpolbul.2014.05.056](https://doi.org/10.1016/j.marpolbul.2014.05.056).
- [12] R. Williams, C. Erbe, E. Ashe, A. Beerman, and J. Smith, "Severity of killer whale behavioral responses to ship noise: A dose-response study," *Mar. Pollut. Bull.*, vol. 79, no. 1/2, pp. 254–260, 2014, doi: [10.1016/j.marpolbul.2013.12.004](https://doi.org/10.1016/j.marpolbul.2013.12.004).
- [13] D. M. Wisniewska et al., "High rates of vessel noise disrupt foraging in wild harbour porpoises (*Phocoena phocoena*)," *Proc. Roy. Soc. B, Biol. Sci.*, vol. 285, no. 1872, pp. 1–10, 2018, doi: [10.1098/rspb.2017.2314](https://doi.org/10.1098/rspb.2017.2314).
- [14] K. R. Sprogis, S. Videsen, and P. T. Madsen, "Vessel noise exposure level drives behavioural responses of humpback whales with implications for whale-watching," *Elife*, vol. 9, Jun. 2020, Art. no. e56760, doi: [10.7554/elife.56760](https://doi.org/10.7554/elife.56760).
- [15] T. A. Nichols, T. W. Anderson, and A. Širović, "Intermittent noise induces physiological stress in a coastal marine fish," *PLoS One*, vol. 10, no. 9, 2015, Art. no. e0139157, doi: [10.1371/journal.pone.0139157](https://doi.org/10.1371/journal.pone.0139157).
- [16] P. L. Tyack, "Implications for marine mammals of large-scale changes in the marine acoustic environment," *J. Mammal.*, vol. 89, no. 3, pp. 549–558, 2008, doi: [10.1644/07-MAMM-S-307R.1](https://doi.org/10.1644/07-MAMM-S-307R.1).
- [17] L. H. McWhinnie, W. D. Halliday, S. J. Insley, C. Hilliard, and R. R. Canessa, "Vessel traffic in the Canadian Arctic: Management solutions for minimizing impacts on whales in a changing northern region," *Ocean Coastal Manage.*, vol. 160, pp. 1–17, 2018, doi: [10.1016/j.ocecoaman.2018.03.042](https://doi.org/10.1016/j.ocecoaman.2018.03.042).
- [18] H. Breeze, V. Nolet, D. Thomson, A. J. Wright, E. Marotte, and M. Sanders, "Efforts to advance underwater noise management in Canada: Introduction to the Marine Pollution Bulletin Special issue," *Mar. Pollut. Bull.*, vol. 178, 2022, Art. no. 113596, doi: [10.1016/j.marpolbul.2022.113596](https://doi.org/10.1016/j.marpolbul.2022.113596).
- [19] A. O. Macgillivray, Z. Li, D. E. Hannay, K. B. Trounce, and O. M. Robinson, "Slowing deep-sea commercial vessels reduces underwater radiated noise," *J. Acoust. Soc. Amer.*, vol. 146, pp. 340–351, 2019, doi: [10.1121/1.5116140](https://doi.org/10.1121/1.5116140).
- [20] G. M. Wenz, "Acoustic ambient noise in the ocean: Spectra and sources," *J. Acoust. Soc. Amer.*, vol. 34, no. 12, pp. 1936–1956, 1962.
- [21] J. G. Lourens and J. A. Du Preez, "Passive sonar ML estimator for ship propeller speed," *IEEE J. Ocean. Eng.*, vol. 23, no. 4, pp. 448–453, Oct. 1998, doi: [10.1109/48.725238](https://doi.org/10.1109/48.725238).
- [22] M. L. Seto, "Application of tonal tracking to ship acoustic signature feature identification," *J. Vib. Acoust. Trans.*, vol. 133, no. 6, 2011, Art. no. 064501, doi: [10.1115/1.4004606](https://doi.org/10.1115/1.4004606).
- [23] S. Yang, Z. Li, and X. Wang, "Ship recognition via its radiated sound: The fractal based approaches," *J. Acoust. Soc. Amer.*, vol. 112, no. 1, pp. 172–177, 2002, doi: [10.1121/1.1487840](https://doi.org/10.1121/1.1487840).
- [24] F. Aulanier, Y. Simard, N. Roy, C. Gervaise, and M. Bandet, "Effects of shipping on marine acoustic habitats in Canadian Arctic estimated via probabilistic modelling and mapping," *Mar. Pollut. Bull.*, vol. 125, no. 1/2, pp. 115–113, 2017, doi: [10.1016/j.marpolbul.2017.08.002](https://doi.org/10.1016/j.marpolbul.2017.08.002).
- [25] Y. Simard, N. Roy, and C. Gervaise, "Passive acoustic detection and localization of whales: Effects of shipping noise in Saguenay–St. Lawrence Marine Park," *J. Acoust. Soc. Amer.*, vol. 123, no. 6, pp. 4109–4117, 2008, doi: [10.1121/1.2912453](https://doi.org/10.1121/1.2912453).
- [26] J. K. Allen, M. L. Peterson, G. V. Sharrard, D. L. Wright, and S. K. Todd, "Radiated noise from commercial ships in the Gulf of Maine: Implications for whale/vessel collisions," *J. Acoust. Soc. Amer.*, vol. 132, pp. EL229–EL235, 2012, doi: [10.1121/1.4739251](https://doi.org/10.1121/1.4739251).
- [27] J. A. A. J. Jannsen, H. Hasenpflug, and M. Janßen, "COSIMAR: Continuous operational signature monitoring awareness and recommendation," in *Proc. Int. Nav. Eng. Conf. Exhib.*, 2018, vol. 14, pp. 1–10, doi: [10.24868/issn.2515-818x.2018.027](https://doi.org/10.24868/issn.2515-818x.2018.027).
- [28] C. Gervaise, F. Aulanier, Y. Simard, and N. Roy, "Mapping probability of shipping sound exposure level," *J. Acoust. Soc. Amer.*, vol. 137, no. 6, pp. EL429–EL435, 2015, doi: [10.1121/1.4921673](https://doi.org/10.1121/1.4921673).
- [29] J. P. Jalkanen, L. Johansson, M. H. Andersson, E. Majamäki, and P. Sigray, "Underwater noise emissions from ships during 2014–2020," *Environ. Pollut.*, vol. 311, 2022, Art. no. 119766, doi: [10.1016/j.envpol.2022.119766](https://doi.org/10.1016/j.envpol.2022.119766).
- [30] L. S. Wang, S. P. Robinson, P. Theobald, P. A. Lepper, G. Hayman, and V. F. Humphrey, "Measurement of radiated ship noise," *Proc. Meetings Acoust.*, vol. 17, no. 1, 2013, Art. no. 070091, doi: [10.1121/1.4792663](https://doi.org/10.1121/1.4792663).
- [31] M. P. Salio, "Numerical assessment of underwater noise radiated by a cruise ship," *Ships Offshore Struct.*, vol. 10, no. 3, pp. 308–327, 2015, doi: [10.1080/17445302.2013.790271](https://doi.org/10.1080/17445302.2013.790271).
- [32] S. C. Wales and R. M. Heitmeyer, "An ensemble source spectra model for merchant ship-radiated noise," *J. Acoust. Soc. Amer.*, vol. 111, no. 3, pp. 1211–1231, 2002, doi: [10.1121/1.1427355](https://doi.org/10.1121/1.1427355).
- [33] ANSI, *ANSI/ASA S12-64: Quantities and Procedures for Description and Measurement of Underwater Sound from Ships – Part 1: General Requirements*. New York, NY, USA: Acoustical Society of America, 2009, doi: [10.1016/0003-6870\(91\)90314-8](https://doi.org/10.1016/0003-6870(91)90314-8).
- [34] International Organization for Standardization, *Underwater Acoustics — Quantities and Procedures for Description and Measurement of Underwater Sound from Ships—Part 2: determination of Source Levels from Deep Water Measurements*, ISO Standard 17208-2:2019, International Organization for Standardization, 2019.
- [35] *Underwater Acoustics – Quantities and Procedures for Description and Measurement of Underwater Sound from Ships – Part 1: Requirements for Precision Measurements in Deep Water Used for Comparison Purposes*, ISO Standard 17208-1:2016, International Organization for Standardization, 2016.
- [36] D. Ross, *Mechanics of Underwater Noise*, 1st ed. New York, NY, USA: Pergamon Press, 1979, doi: [10.1017/S0022112079210677](https://doi.org/10.1017/S0022112079210677).
- [37] E. E. Ungar and D. Ross, "Vibrations and noise due to piston-slap in reciprocating machinery," *J. Sound Vib.*, vol. 2, no. 2, pp. 132–146, 1965.
- [38] P. T. Arveson and D. J. Venditti, "Radiated noise characteristics of a modern cargo ship," *J. Acoust. Soc. Amer.*, vol. 107, no. 1, pp. 118–129, 2000, doi: [10.1121/1.428344](https://doi.org/10.1121/1.428344).
- [39] M. F. McKenna, S. M. Wiggins, and J. A. Hildebrand, "Relationship between container ship underwater noise levels and ship design, operational and oceanographic conditions," *Sci. Rep.*, vol. 3, 2013, Art. no. 1760, doi: [10.1038/srep01760](https://doi.org/10.1038/srep01760).
- [40] M. V. Trevoror, "Evidence for non-Rayleigh characteristics in ship underwater acoustic signatures," *J. Acoust. Soc. Amer.*, vol. 149, no. 4, pp. 2270–2282, 2021, doi: [10.1121/10.0004132](https://doi.org/10.1121/10.0004132).
- [41] L. Gilroy, "Ship noise management and the ORCA class of ships," *Mar. Pollut. Bull.*, vol. 174, 2022, Art. no. 113196, doi: [10.1016/j.marpolbul.2021.113196](https://doi.org/10.1016/j.marpolbul.2021.113196).
- [42] M. A. Ainslie et al., "International harmonization of procedures for measuring and analyzing of vessel underwater radiated noise," *Mar. Pollut. Bull.*, vol. 174, 2022, Art. no. 113124, doi: [10.1016/j.marpolbul.2021.113124](https://doi.org/10.1016/j.marpolbul.2021.113124).
- [43] I. Karasalo et al., "Estimates of source spectra of ships from long term recordings in the Baltic sea," *Front. Mar. Sci.*, vol. 4, 2017, Art. no. 164, doi: [10.3389/fmars.2017.00164](https://doi.org/10.3389/fmars.2017.00164).
- [44] D. Tollefsen, W. S. Hodgkiss, S. E. Dosso, J. Bonnel, and D. P. Knobles, "Probabilistic estimation of merchant ship source levels in an uncertain shallow-water environment," *IEEE J. Ocean. Eng.*, vol. 47, no. 3, pp. 647–656, Jul. 2022, doi: [10.1109/JOE.2021.3113506](https://doi.org/10.1109/JOE.2021.3113506).
- [45] C. Chion, D. Lagrois, and J. Dupras, "A meta-analysis to understand the variability in reported source levels of noise radiated by ships from opportunistic studies," *Front. Mar. Sci.*, vol. 6, pp. 1–14, 2019, doi: [10.3389/fmars.2019.00714](https://doi.org/10.3389/fmars.2019.00714).
- [46] N. Shahjahan, D. R. Barclay, and Y.-T. Lin, "Quantifying the contribution of ship noise to the underwater sound field," *J. Acoust. Soc. Amer.*, vol. 148, no. 6, pp. 3863–3872, 2020, doi: [10.1121/10.0002922](https://doi.org/10.1121/10.0002922).
- [47] L. M. Gray and D. S. Greeley, "Source level model for propeller blade rate radiation for the world's merchant fleet," *J. Acoust. Soc. Amer.*, vol. 67, no. 2, pp. 516–522, 1980, doi: [10.1121/1.383916](https://doi.org/10.1121/1.383916).
- [48] F. Traverso, T. Gaggero, E. Rizzuto, and A. Trucco, "Spectral analysis of the underwater acoustic noise radiated by ships with controllable pitch propellers," in *Proc. OCEANS— Genova*, 2015, pp. 1–6, doi: [10.1109/OCEANS-Genova.2015.7271483](https://doi.org/10.1109/OCEANS-Genova.2015.7271483).
- [49] S. Turkmen, B. Aktas, M. Atlar, N. Sasaki, R. Sampson, and W. Shi, "On-board measurement techniques to quantify underwater radiated noise level," *Ocean Eng.*, vol. 130, pp. 166–175, 2017, doi: [10.1016/j.oceaneng.2016.11.070](https://doi.org/10.1016/j.oceaneng.2016.11.070).
- [50] D. J. Venditti and P. T. Arveson, "Ten challenges in measuring and reporting ship noise levels," *JASA Exp. Lett.*, vol. 2, no. 3, 2022, Art. no. 036801, doi: [10.1121/10.0009726](https://doi.org/10.1121/10.0009726).

- [51] D. J. Vendittis and P. Arveson, "Errors due to Doppler shift in measured levels from a moving ship," *J. Washington Acad. Sci.*, vol. 107, no. 1, pp. 29–34, 2021.
- [52] W. Huang, D. Wang, H. Garcia, O. Godø, and P. Ratilal, "Continental shelf-scale passive acoustic detection and characterization of diesel-electric ships using a coherent hydrophone array," *Remote Sens.*, vol. 9, no. 8, 2017, Art. no. 772, doi: [10.3390/rs9080772](https://doi.org/10.3390/rs9080772).
- [53] M. Gassmann, S. M. Wiggins, and J. A. Hildebrand, "Deep-water measurements of container ship radiated noise signatures and directionality," *J. Acoust. Soc. Amer.*, vol. 142, no. 3, pp. 1563–1574, 2017, doi: [10.1121/1.5001063](https://doi.org/10.1121/1.5001063).
- [54] M. V. Trevorrow, B. Vasiliev, and S. Vagle, "Directionality and maneuvering effects on a surface ship underwater acoustic signature," *J. Acoust. Soc. Amer.*, vol. 124, no. 2, pp. 767–778, 2008, doi: [10.1121/1.2939128](https://doi.org/10.1121/1.2939128).
- [55] J. S. Park, D. Kang, and S. Cho, "Noise directionality estimated using ship tracking data in the Southern Sea of Korea," *Jpn. J. Appl. Phys.*, vol. 57, no. 7, 2018, Art. no. 07LG06, doi: [10.7567/JJAP.57.07LG06](https://doi.org/10.7567/JJAP.57.07LG06).
- [56] G. J. Heard, B. McArthur, and G. Inglis, "Overview of the technical results of the Northern Watch Project," Def. Res. Develop. Canada, Ottawa, ON, Canada, 2016.
- [57] J. Dawson, L. Pizzolato, S. E. L. Howell, L. Copland, and M. E. Johnston, "Temporal and spatial patterns of ship traffic in the Canadian Arctic from 1990 to 2015," *Arctic*, vol. 71, no. 1, pp. 15–26, 2018, doi: [10.14430/arctic4698](https://doi.org/10.14430/arctic4698).
- [58] S. P. Pecknold and C. M. Binder, "A comparison of acoustic propagation models for Canadian Arctic underwater sentinel experimentation (CAUSE)," Def. Res. Develop. Canada, Ottawa, ON, Canada, Sci. Rep. DRDC-RDDC-2020-R113, 2020.
- [59] S. P. Pecknold, N. Pelavas, and G. J. Heard, "Measurements and modeling of transmission loss variability in Barrow Strait," in *Proc. Meetings Acoust.*, 2013, vol. 19, doi: [10.1121/1.4800589](https://doi.org/10.1121/1.4800589).
- [60] K. Kyle, "Hybrid-powered electric cruise ship navigates Northwest passage," *CBC News.*, Accessed: Sep. 30, 2019. [Online]. Available: <http://www.cbc.ca/news/canada/north/amundsen-arctic-hybrid-cruise-1.5290158>
- [61] R. G. Vaughan, N. L. Scott, and D. R. White, "The theory of bandpass sampling," *IEEE Trans. Signal Process.*, vol. 39, no. 9, pp. 1973–1984, Sep. 1991, doi: [10.1109/78.134430](https://doi.org/10.1109/78.134430).
- [62] D. Thomson and D. R. Barclay, "Individual horizontal array elements as windows to estimating ship radiated noise signature lobing patterns," *J. Acoust. Soc. Amer.*, vol. 146, no. 4, Oct. 2019, Art. no. 3062, doi: [10.1121/1.5137628](https://doi.org/10.1121/1.5137628).



Dugald J. M. Thomson (Member, IEEE) received the B.Eng. degree in electrical engineering from the Royal Military College of Canada, Kingston, ON, Canada, in 2004, and the M.Sc. degree in ocean acoustics from the University of Victoria, Victoria, BC, Canada, in 2012. He is currently working toward the Ph.D. degree in underwater acoustics with the Oceanography Department, Dalhousie University, Halifax, NS, Canada.

He is a Major in the Royal Canadian Air Force, a past recipient of the Fessenden Prize in Underwater Acoustics, a Royal Canadian Navy Athlete of the Year, and a past chair of the Maritime Acoustic Symposium. His research interests include nonlinear properties of liquid seawater in gravitational surface waves or converting gravitational potential energy into its more useful kinetic form in British Columbia's Coast Mountains.



David R. Barclay (Member, IEEE) received the B.Sc. (Hons.) degree in physics with a minor in music technology from McGill University, Montreal, QC, Canada, in 2005, and the Ph.D. degree in oceanography from the Scripps Institution of Oceanography, University of California, San Diego, La Jolla, CA, USA, in 2011.

He was a Deep Ocean Exploration Institute postdoctoral scholar and an Office of Naval Research postdoctoral fellow in Ocean Acoustics at the Woods Hole Oceanographic Institution, as well as a postdoctoral researcher at the Memorial University of Newfoundland. He is currently an Associate Professor and the Canada Research Chair with the Ocean Technology Systems, Department of Oceanography, Dalhousie University, Halifax, NS, Canada.

Dr. Barclay is a Member of the Acoustical Society of America and an Associate Editor in acoustical oceanography for the *JASA Express Letters* and *IEEE JOURNAL OF OCEANIC TECHNOLOGY*.